Electronic Supplementary Material (ESI) for Nanoscale.

Supporting Information

Me-Graphene: A Graphene Allotrope with Near Zero Poisson's Ratio, Sizeable Band Gap, and High Carrier Mobility

Zhiwen Zhuo,[a] Xiaojun Wu,[a,b,*] and Jinlong Yang[a,b]

[a] Hefei National Laboratory for Physical Sciences at the Microscale, School of Chemistry and Materials Sciences, CAS Key Laboratory of Materials for Energy Conversion, and CAS Center for Excellence in Nanoscience, University of Science and Technology of China, Hefei, Anhui 230026, China

[b] Synergetic Innovation of Quantum Information & Quantum Technology, University of Science and Technology of China, Hefei, Anhui 230026, China

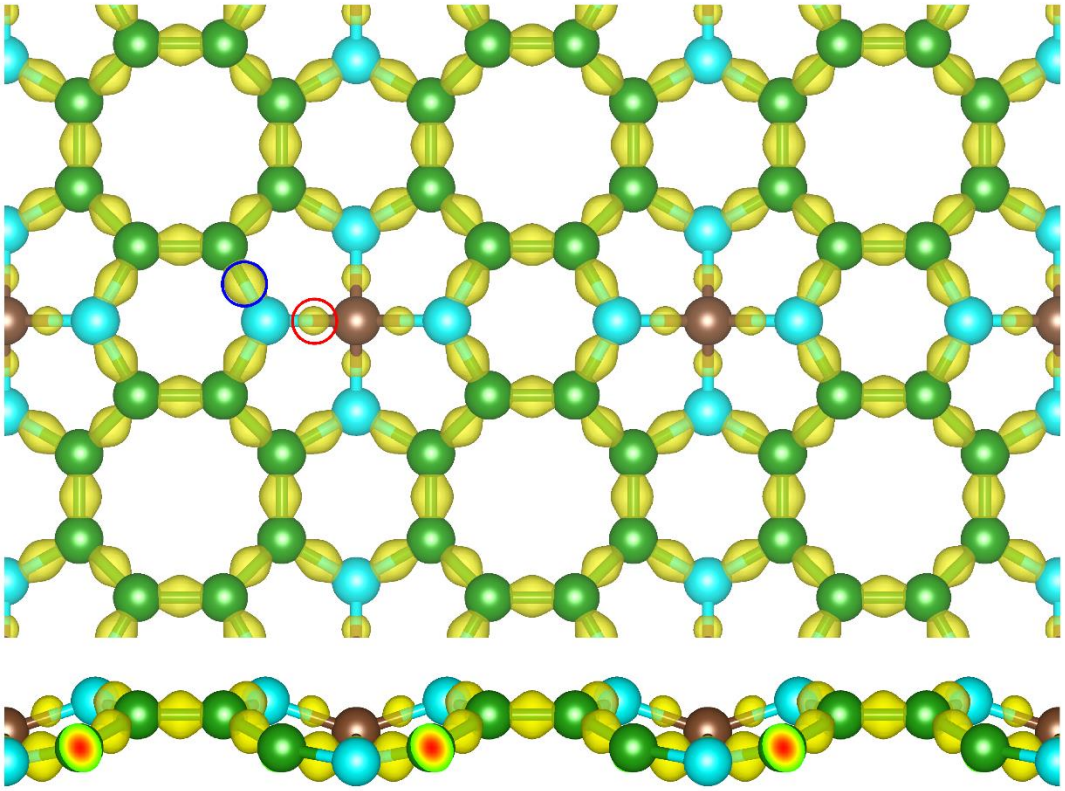

Fig. S1 Deformation charge density of Me-graphene (isosurface is 0.03 e/Bohr^3)

The deformation charge can unveil the bonding degree with its value, larger and thicker density distribution in yellow color (electron density increase zone) indicates high bonding degree that introduced by delocalized π bond with existence of the highly localized σ bonding. The similar density over all sp^2 carbon (blue circle) indicates the widely delocalized π bond, while the bonding of sp^3 carbon (red circle) is the highly localized σ bonding, which has smaller density cloud volume with same isosurface. Note that the electron density decease zone (in blue color indeed) is too small to see with setting of isosurface of 0.03 e/Bohr^3.

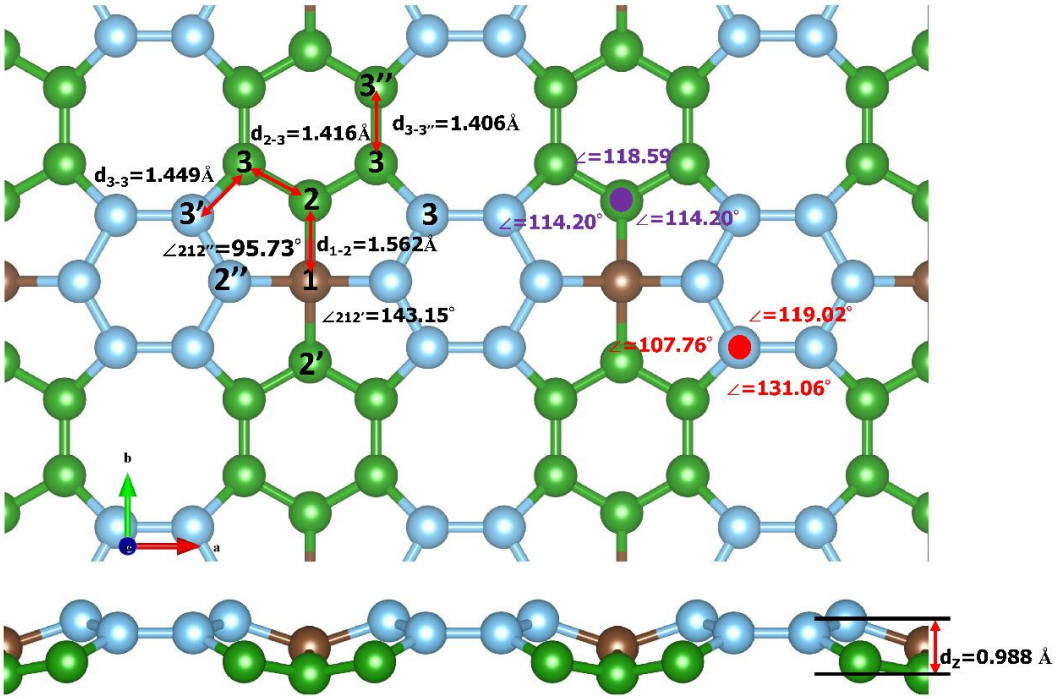

Fig. S2 Structure details of Me-graphene

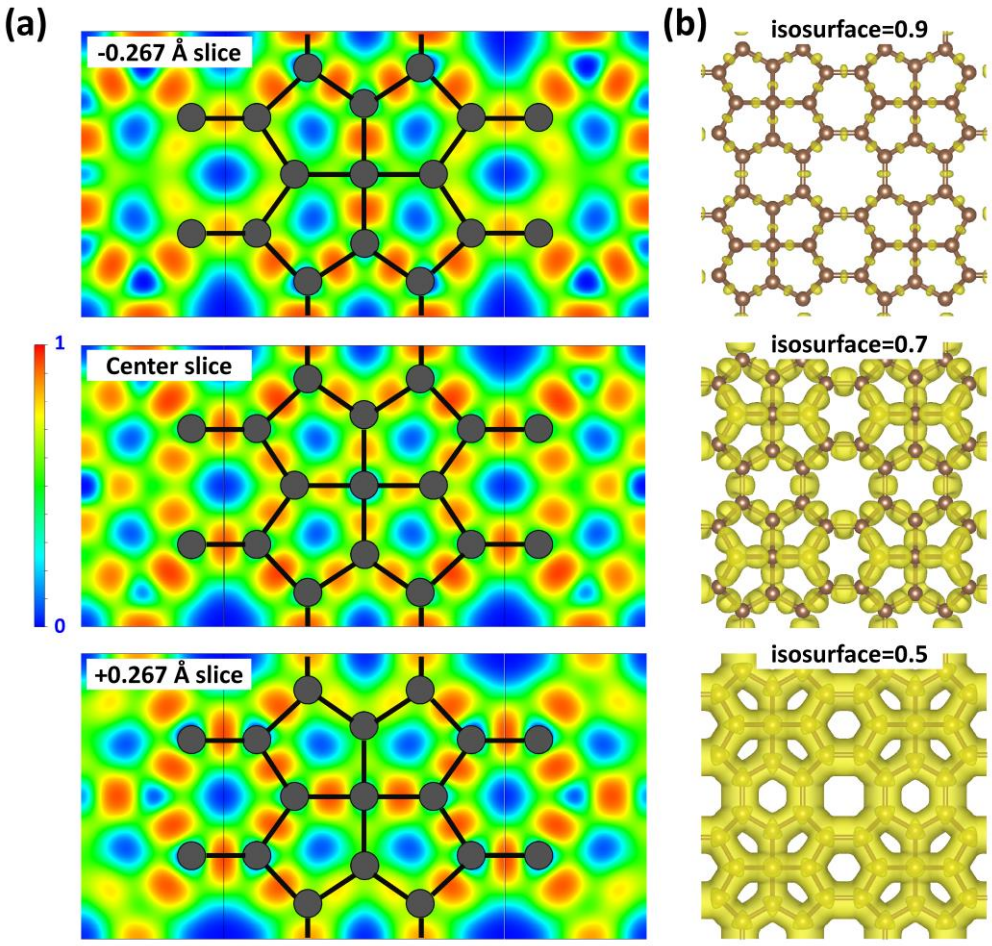

Fig. S3 ELF of Me-graphene: (a) slice at different positions, (b) with different isosufaces

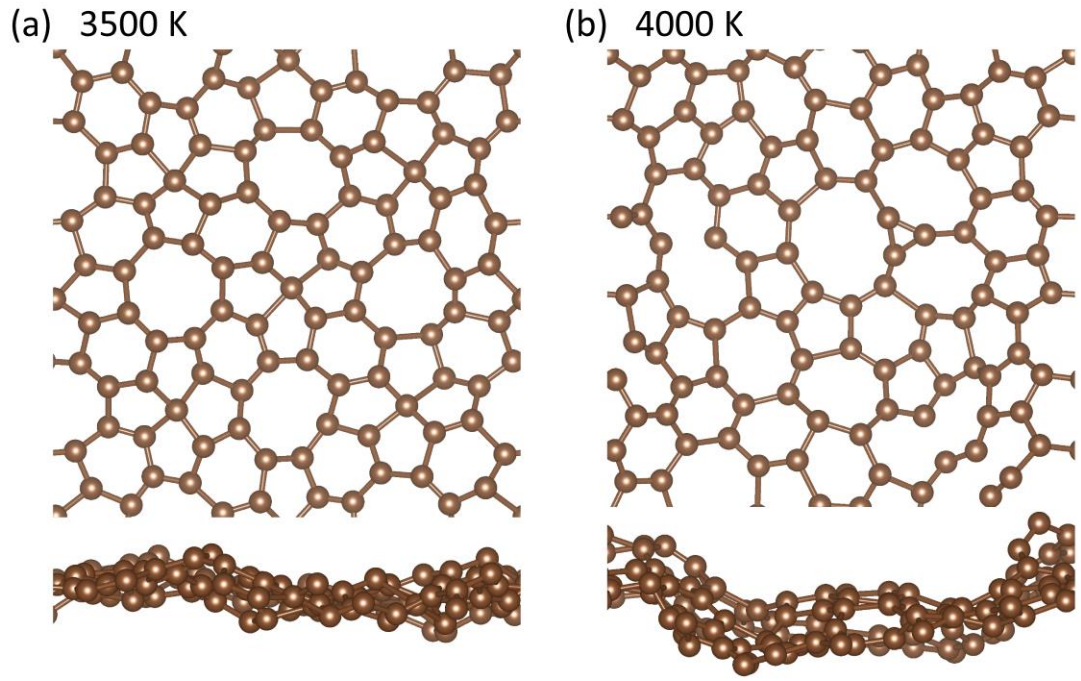

Fig. S4 Snapshot of structure (Top view and side view) of Me-graphene at temperature of (a) 3500K and (b) 4000 K after 5ps BOMD simulation.

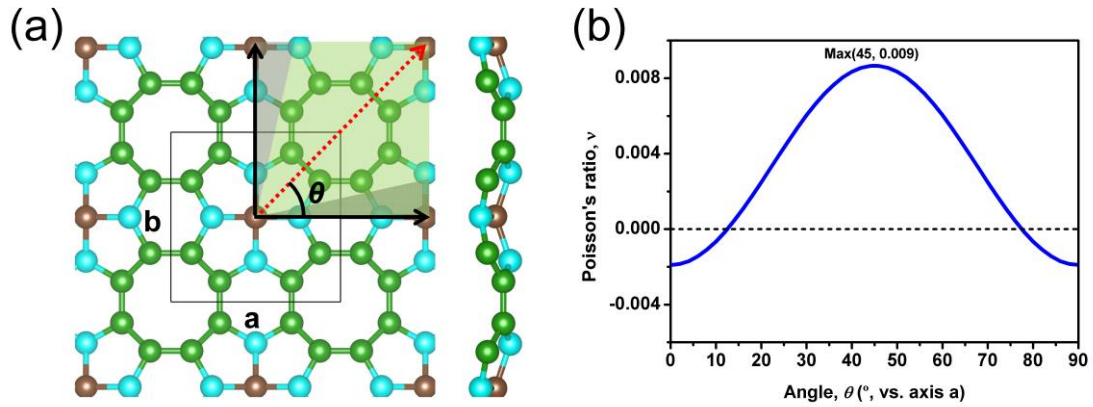

Fig. S5 (a) The illustration of Poisson's ratio distribution in different directions in x-y plane of Me-graphene. (The gray angle region represents negative value while the green angle regions represent positive value. And the blue arrow is the specified direction ϑ.) (b) The variation of Poisson's ratio (ν) value in different directions (represented by angle ϑ, vs. axis **a**) in *x*-*y* plane of Me-graphene. Duo to the limitation of symmetry, only two concise angle regions (0-45 degree and 45-90 degree, respectively) with a total angle region ranging from 0 to 90 degree are shown.

Direction-depended Poisson's ratio calculation. The value of ν(ϑ) can be calculated via equations reported in previous work[1] as listed as below:

$$\nu(\theta) = \frac{(\nu_{xy}\cos^4\theta - d_1\cos^2\theta\sin^2\theta + \nu_{xy}\sin^4\theta)}{(\cos^4\theta + d_2\cos^2\theta\sin^2\theta + d_3\sin^4\theta)}, \quad \text{(ES1)}$$

where, ϑ is the included angle between axis *x* (here, axis *x* is corresponding to axis **a** while axis *y* is axis **b** in Me-graphene) and specified direction ϑ to apply strain, and ν_{xy}, d_1, d_2 and d_3 are defined as:

$$\nu_{xy} = C_{21}/C_{22} = C_{12}/C_{22}, \quad \text{(ES2)}$$

$$d_1 = \frac{C_{11}}{C_{22}} + 1 - \frac{C_{11}C_{22} - C_{12}^2}{C_{22}C_{66}} \quad \text{(ES3)}$$

$$d_2 = -(2\frac{C_{12}}{C_{22}} - \frac{C_{11}C_{22} - C_{12}^2}{C_{22}C_{66}}) \quad \text{(ES4)}$$

$$d_3 = \frac{C_{11}}{C_{22}} \quad \text{(ES5)}$$

Here, the C_{11}, C_{22}, C_{12} and C_{66} are 210, 210, -0.4, and 103 N/m, respectively. The calculated value of ν(ϑ) is ν(ϑ = 0°) = -0.002, ν(ϑ = 12.5°) = 0, ν(ϑ = 45°) = 0.009, ν(ϑ = 77.5°) = 0 and ν(ϑ = 90°) = -0.002. In the concise angle region (0 to 45 degree), the angle interval with negative value is from 0 to 12.5 degree (as 27.8 % for full directions in *x*-*y* plane), while the angle interval with positive value is from 12.5 to 45 degree (as 72.2 % for full directions in x-y plane). And there is one ideal ZPR at ϑ = 12.5° for one concise angle region. More important, all values are less than |0.01|, suggesting the highly near ZPR in Me-graphene.

GW calculation. The GW calculations were carried out in the framework of DFT-GW scheme by VASP package with the projector-augmented wave method (PAW) and the Perdew-Burke-Ernzerhof (PBE) exchange correlation functional. This GW calculations were performed in a partially self-consistent way (the so-called GW0 approach).[2] In order to obtain the accurate GW band gaps, it is vital to carefully examine the convergence of the quasiparticle bands in the GW calculations.

To test the GW method is computed correctly with reasonable output, the silicon bulk has been checked, of which the GW band gap of silicon (k: 8×8×8, two atoms in unit cell, empty band number was 36 (NBANDS = 40), the energy cutoff for the response functions was 150 eV) has been calculated to be 1.09 eV, well agreed with the experiment result (1.1 eV)[3].

For 2D system, generally, GW band gap is affected by empty band number (N), k-points (n×n) and the separation distance (L_z) in computation.

However, as well known, GW calculation is highly expensive to cost computation resource, especially its ultra-high memory occupation. To obtain an acceptable band gap with reasonable accuracy within limited computation resource, several approximations are applied: (a) The GW calculations were performed in a partially self-consistent way (GW0 approach) to cut down the computation cost; (b) Since the GW band gap (GWBG) converges as $1/L_z$,[4,5] a limit gap can be extrapolated with the infinite L_z, of which L_z of 10, 12, 15, 20, 25 Å are applied; (c) the ratio of band gap to k-points grid, GWBG(dense k-point)/GWBG(low k-point), possess same convergence limit for different L_z.

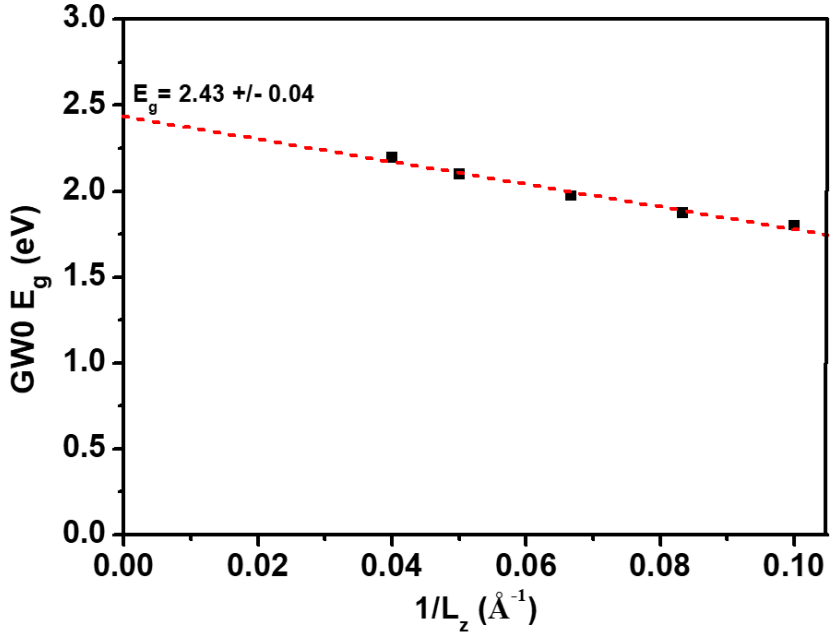

Fig. S6 GW0 band gap depended on L_z to extrapolate the bang gap limit (k: 4×4×1)

First, we have tested some convergences: (i) the energy cutoff for the response functions was set to be 150 eV (ΔE_g = 0.007 eV, vs. 300 eV); (ii) empty band number (N) was set to be 214 (NBANDS = 240); (iii) k-point is 20×20×1 (ΔE_g = 0.008 eV, vs. 18×18×1). Based on (b), GWBG with different Lz in low k-ponit (4×4×1) is carried out to extrapolate the bang gap limit for low k-point situation with a limit GW E_g of 2.43 +/- 0.037 eV, as shown in Fig. S6. Then, based on (c), the GWBG(dense k-point)/GWBG(low k-point) convergence limit is extrapolated, as shown in Table S1.

Table S1. GW band gap value depended on L_z (Å) and k-points. (N=54, NBANDS = 80)

	L_z=10	L_z=12	L_z=15	L_z=20
4×4	1.853	1.936	2.041	2.170
6×6	1.691	1.746	1.821	1.963
8×8	1.645	1.697	1.762	1.878
10×10	1.622	1.684	1.757	-*
E_g(6×6)/E_g(4×4)	0.913	0.902	0.892	0.905
E_g(8×8)/E_g(4×4)	0.888	0.876	0.863	0.865
E_g(10×10)/E_g(4×4)	0.876	0.870	0.861	-*

* Failure occurred due to computer memory limit.

As shown in Table S1, the GWBG(dense k-points)/GWBG(low k-points) highly converges to a constant with the increase of L_z.

Thus an equation can be concluded, (as approximation (c)), listed as below:

$$\frac{E_g(k{:}n\times n, L_z{=}I)}{E_g(k{:}m\times m, L_z{=}I)} = \frac{E_g(k{:}n\times n, L_z{=}J)}{E_g(k{:}m\times m, L_z{=}J)} \quad \text{(ES6)}$$

Within our computation limit, L_z = 10 Å can be carried out up to k points of 20×20,

$$\frac{E_g(k{:}20\times 20, L_z{=}10)}{E_g(k{:}4\times 4, L_z{=}10)} = \frac{E_g(k{:}20\times 20, L_z{=}\infty)}{E_g(k{:}4\times 4, L_z{=}\infty)} \quad \text{(ES7)}$$

Where $E_g(k{:}\,20\times 20, L_z = 10)$ is 1.511 eV, $E_g(k{:}\,4\times 4, L_z = 10)$ is 1.801 eV, $E_g(k{:}\,4\times 4, L_z = \infty)$ is 2.43 +/- 0.037 eV.

And the equation can be adapted as below:

$$\frac{E_g(k{:}20\times 20, c{=}\infty)}{E_g(k{:}4\times 4, c{=}\infty)} = 0.839 \quad \text{(ES8)}$$

Thus, the accurate estimated GWBG of Me-graphene is calculated to be 2.04 +/- 0.03 eV.

Structure change and band gap under biaxial strain: The change of structure and properties under biaxial strain ranging from -5% to +5% are investigated. The change of band lengths and bond angle is shown in Fig. S7. Among them, d_{z2} (height difference in direction ***z***) change outstandingly in the strain range with Δd_{z2} of 0.45 Å, and the change degree of $d1$ (the bond length between sp^3- and sp^2- carbon atoms) is much smaller but still secondly obvious with Δd_1 of 0.14 Å. There is a direct-indirect band gap transition between -3% and -2%, of which band gap is direct type (M → M) from -5% to -3% while it is indirect type (Γ → M) from -2% to +5%, as shown in Fig. 4b&c in main text. This results from the lowest unoccupied state (LUS) at Γ, which is the CBM at 0% strain, is quite sensitive to strain but the highest occupied state (HOS) HOS at Γ and the HOS and LUS at M are not, as shown in Fig. 4c in main text. The partial charge density distribution of the HOS and LUS at Γ and M are shown in Fig. S8. As shown, the LUS at Γ, which mainly contributed by the neighbor C_3-p_z coupling, is sensitive to the change of d_3 and d_{z2}. And the d_{z2} changes quickly under strain to adjust the p_z-p_z overlap from weak at -5% to strong at +5% to sharply shift the energy level. At the meantime, the changes of p_z-p_z coupling of the HOS at Γ, and the HOS and LUS at M are all so slight that the strain-sensitive LUS at Γ switches the band gap between direct and indirect conveniently. In general, the band gap turns from 2.62/1.60/1.04 (at -5%) to to 1.24/0.54/0.16 eV (+5%) with GW0/HSE06/PBE, as shown in Table S2.

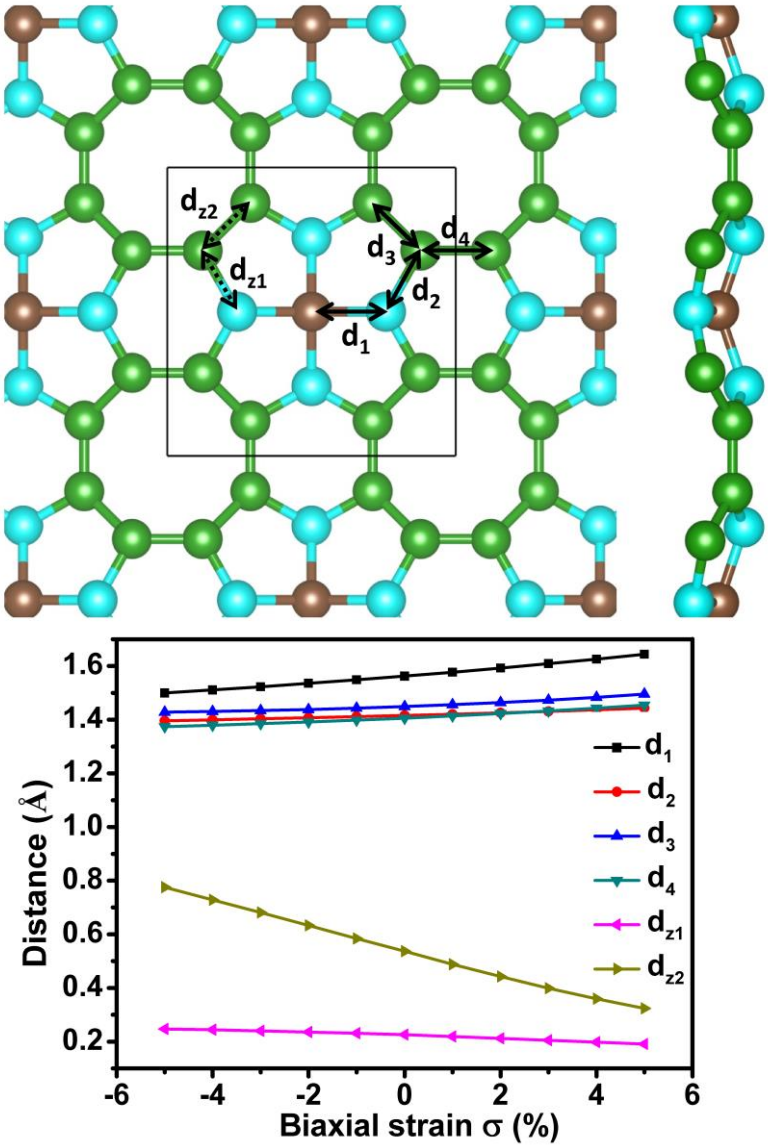

Fig. S7 Specific bond length and highness change under biaxial strain from -5% to +5%

Table S2. Band gap of Me-graphene under different biaxial strain from -5% to +5%.

Strain	PBE (eV)	HSE06 (eV)	GW0 (eV)	Type
-5	1.04	1.60	2.62	M→M
-4	1.04	1.60	2.55	M→M
-3	1.06	1.62	2.57	M→M
-2	0.95	1.43	2.49	M→Γ
-1	0.79	1.25	2.27	M→Γ
0	0.65	1.08	2.04	M→Γ
1	0.51	0.94	1.82	M→Γ
2	0.40	0.80	1.63	M→Γ
3	0.30	0.69	1.46	M→Γ
4	0.22	0.61	1.33	M→Γ
5	0.16	0.54	1.24	M→Γ

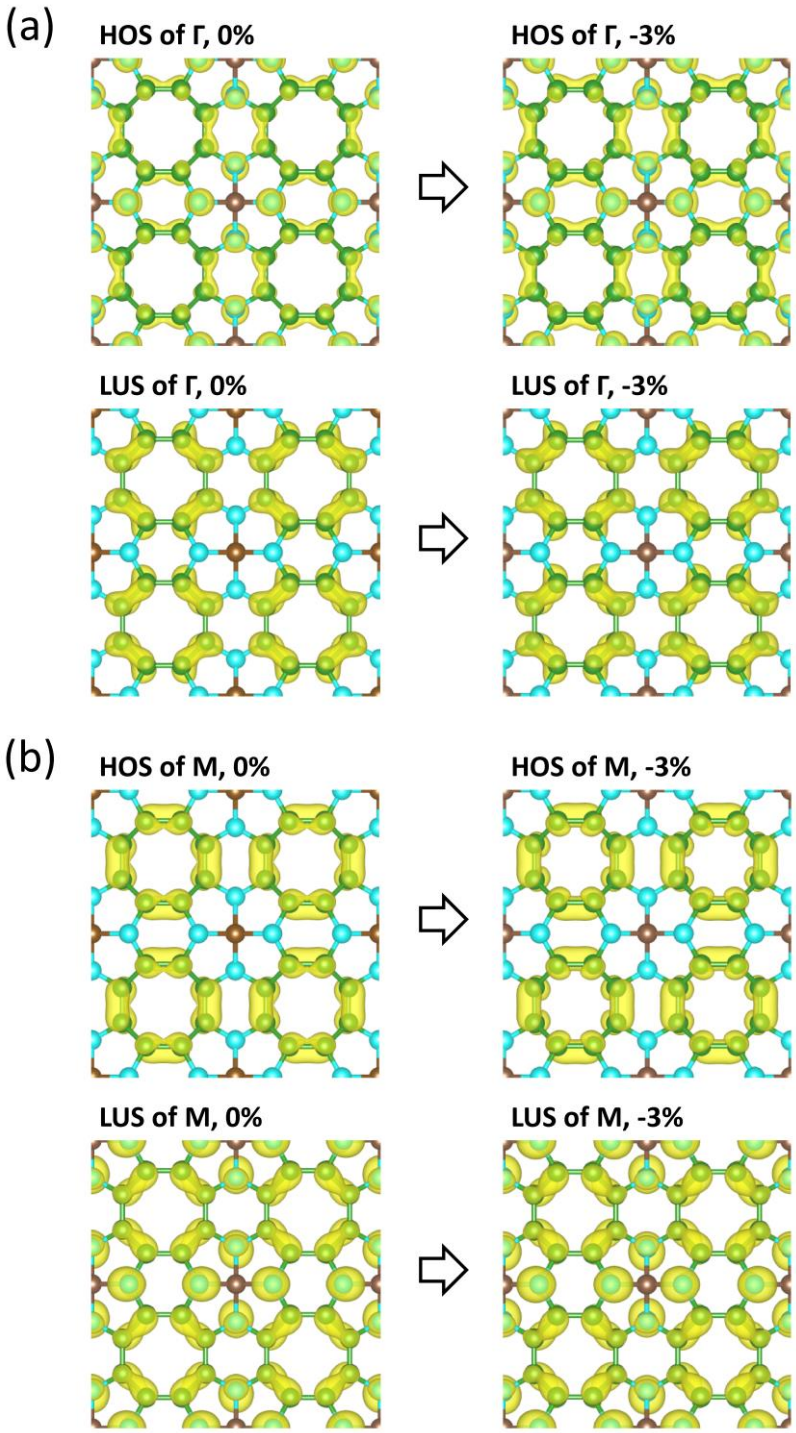

Fig. S8 The partial charge density of specific state at specific k point. (a) The highest occupied state (HOS) and the lowest unoccupied state (LUS) at Γ under biaxial strain of 0% and -3%. (b) The HOS and the LUS at M under biaxial strain of 0% and -3%.

Exciton binding energy. Ordinary DFT method has no consideration on exciton effects in calculation to make their prediction on optical property unreliable. There are ways to estimate the exciton binding energy (E_b), including not just computation with consideration of the electron-hole interaction, such as GW-BSE,[6] but also the relationship between GW band gap and exciton binding energy E_b, which are concluded rules by data fitting, even some methods highly consisted with GW-BSE on pure data collection. In practice, since the GW-BSE calculation is highly expensive in computation resource required harsh hardware conditions, low cost and convenient method to obtain reasonable energy with acceptable value is strongly desired.

Based on previous studies,[7,8] the exciton binding energy is highly near-linear to their GW band gap, $E_b = 0.21*E_g(GW0) + 0.40$, when the E_g is no less than about 1 eV within forced linearly fitting. Thus, the exciton binding energy can conveniently be estimated. For Me-graphene here, E_g (GW) = 2.04 eV with estimated exciton binding energy E_b of 0.83 eV, that the optical band gap of Me-graphene is estimated to be 1.21 eV, comparable to HSE06 value (1.08 eV). Based on the narrow difference on optical band gap, the optical properties carried out with HSE06 instead of GW-BSE is reasonable and acceptable for Me-graphene, especially which is more computation practical.

Carrier mobility calculation. Based on the deformation potential theory of Bardeen and Shockley,[9,10] the carrier mobility in direction α (α = a(x), b(y)) of each band μ_α of 2D structure is defined as,

$$\mu_\alpha = \frac{e\hbar^3 C_\alpha}{k_B T m_\alpha^* m_d (E_{l\alpha})^2} \quad \text{(ES9)}$$

where C_α, k_B, T, m^*_α, and $E_{l\alpha}$ are the elastic constant in direction α, the Boltzmann constant, temperature (set as 300 K, here), effective mass in direction α, and deformation potential for α, respectively. m_d is the average of effective mass in direction **a** and direction **b**, defined as $m_d = (m^*_a m^*_b)^{1/2}$. Deformation potential $E_{l\alpha}$ is defined by $E_{l\alpha} = (\Delta E)/(\Delta l/l)$, where ΔE and $\Delta l/l$ represent the change of band energy and strain in that direction, compared to constant l, respectively. And the step $\Delta l/l$ is 0.2% and strain range is from -0.6% to 0.6% to fitting an average $E_{l\alpha}$.

Here, only the axial directions are considered, of which direction **b** is equal to direction **a** in symmetry. The calculated result is shown in Table S3. The effective mass of **a** (or **b**) at CBM and VBM of Me-graphene ($m^*_{\mathrm{VBM,a}}$ and $m^*_{\mathrm{CBM,a}}$) are -0.18 and 0.68 m_e, respectively. The deformation potential $E_{\mathrm{l,VBM,a}}$ and $E_{\mathrm{l,CBM,a}}$ is -0.93 and -7.86 eV, respectively, agreed with that the energy level of the CBM is sensitive but the VBM is not. At room temperature (300 K), the calculated carrier mobility of μ_{h} and μ_{e} in direction **a** is 1.60×10^5 and 157 $cm^2V^{-1}s^{-1}$, respectively.

Table S3. Mobility calculation details parameters of hole (h) and electron (e) in direction **a** and **b**. ($C_a = C_b = C_{11} = 210$ N/m)

	h(**a**)	h(**b**)	e(**a**)	e(**b**)
Effective mass (m_e)	-0.18	-0.18	0.68	0.68
m_d (m_e)*	0.18	0.18	0.68	0.68
E_l (eV)	-0.93	-0.93	-7.86	-7.86
μ ($cm^2V^{-1}s^{-1}$)	1.60×10^5	1.60×10^5	157	157

* m_e is the static mass of electron.

To understand the contribution to the mobility difference between electron and hole, the equation ES9 can be simplified for Me-graphene as below:

$$\mu_{\alpha} \propto \frac{1}{m_{\mathrm{a}}^{*2} \mathrm{E_{l,a}}^{2}} \tag{ES10}$$

The difference of effective mass of $m^*_{\mathrm{VBM,a}}$ and $m^*_{\mathrm{CBM,a}}$ and deformation potential $E_{\mathrm{l,VBM,a}}$ and $E_{\mathrm{l,CBM,a}}$ decides the difference of mobility for different carriers.

For the contribution of effective mass and deformation potential, effective mass part $((m^*)^{-2})$ of hole/electron is $(1/0.18^2)/(1/0.68^2)$=14.27 times, while deformation potential part (E_l^{-2}) of hole/electron is $(1/0.93^2)/(1/7.86^2)$=71.43 times. Thus, the significantly smaller effective mass as well as deformation potential of hole than electron results in the outstanding difference mobility for carrier hole and electron, as about 10^3 times.

Understanding of deformation potential difference between electron and hole. As Fig. S9 shown, the partial density of VBM locates between atom pairs of (1,2), (3,4), (5,6), and (7,8), of which the bond lengths are denoted as d_{1a} ('a' represent it parallel to axial **a**) and d_{1b} ('b' represent it parallel to axial **b**) within a typical p_z-p_z coupling, respectively, while the partial density of CBM locates between atom pairs (2,3), (4,5), (6,7), and (8,1), denoted as d_2 within typical p_z-p_z coupling/hybridization as well, of which there is position difference in direction z between atom pairs of (2,3), (4,5), (6,7), and (8,1), denoted as d_{z2}, which represents the highness difference between atoms of each pair. And the d_{z2} can affect the p_z-p_z orbital overlap (Fig. S9f) as well as bond length do (Fig. S9e).

Based on the partial density of VBM locates between atom pairs of (1,2), (3,4), (5,6), and (7,8), the partial density zone (PDZ) of each pair can be labelled as $n_e(1,2)$, $n_e(3,4)$, $n_e(5,6)$, and $n_e(7,8)$ with energy of $E(n_e(1,2))$, $E(n_e(3,4))$, $E(n_e(5,6))$ and $E(n_e(7,8))$, respectively, of which the total energy of partial density zone of VBM is the summation of all of the pairs, listed as below:

$$E_{VBM} = E(n_e(1,2)) + E(n_e(3,4)) + E(n_e(5,6)) + E(n_e(7,8)) \tag{ES11}$$

Where all PDZs basically determined by the distance between atoms of each pair (d_{1a} or d_{1b}). Thus, ES11 can be described as equation listed below:

$$E_{VBM}(d_{1a},d_{1b}) = E(d_{1a}) + E(d_{1a}) + E(d_{1b}) + E(d_{1b}) = 2E(d_{1a}) + 2E(d_{1b}) \tag{ES12}$$

Similarly, the total energy of PDZ of CBM can be described by equation listed as below:

$$E_{CBM} = E(n_e(2,3)) + E(n_e(4,5)) + E(n_e(6,7)) + E(n_e(8,1)) \tag{ES13}$$

Where, the energy of each PDZ involves not just distance between atoms in each pair (denoted as d_2) but also the highness difference (denoted as d_{z2}), which can affect the p_z-p_z orbitals overlap in π bonding.

Thus, ES13 can be described as new equation listed below:

$$E_{CBM}(d_2,d_{z2}) = E(d_2,d_{z2}) + E(d_2,d_{z2}) + E(d_2,d_{z2}) + E(d_2,d_{z2}) = 4E(d_2,d_{z2}) \tag{ES14}$$

Where all pairs have the same kind of bond length, the same shape of PDZ as well as the same response to the strain in symmetry.

Interestingly, due to the linear relationship between PDZ energy of VBM (or CBM) and applied strain σ_a (within narrow range of σ_a), as shown in Fig. S10a, E_{CBM} and E_{CBM} can be described as:

$$E_{VBM} = k_{VBM}\sigma_a \quad \text{(ES15)}$$

$$E_{CBM} = k_{CBM}\sigma_a \quad \text{(ES16)}$$

Where, the k_{VBM} and k_{VBM} are constant coefficients.

Due to the distance and highness d_{1a}, d_{1b}, d_2 and d_{z2} are all in linear relationship with applied strain as well, as shown in Fig. S10b-d, the $E_{VBM}(d_{1a},d_{1b})$ and $E_{CBM}(d_2,d_{z2})$ can transform into equations listed as below:

$$E_{VBM}(d_{1a},d_{1b}) = 2k_{1a}d_{1a} + 2k_{1b}d_{1b} \quad \text{(ES17)}$$

$$E_{CBM}(d_2,d_{z2}) = 4k_2d_2 + 4g_{z2}d_{2z} \quad \text{(ES18)}$$

Where, k_{1a}, k_{1b}, k_2 is coefficient depended on distance of each atom pair (as well as the C=C bond length), and g_{z2} is depended on the highness difference of each pair.

If we roughly considered the all C=C bond performs similar or same in response, due to their close bond length and the high covalence in Me-graphene, there is $k_{1a}=k_{1b}=k_2$ (unified as k_π), then

$$E_{VBM}(d_{1a},d_{1b}) = 2k_\pi(d_{1a} + d_{1b}) \quad \text{(ES19)}$$

$$E_{CBM}(d_2,d_{z2}) = 4k_\pi d_2 + 4g_{z2}d_{2z} \quad \text{(ES20)}$$

Based on the result shown as Fig. S9d, there is $2(\Delta d_{1a} + \Delta d_{1b}) \approx 4\Delta d_2$. Thus, the main difference between deformation potential of $E_{l,VBM,a}$ and $E_{l,CBM,a}$ would be

$$E_{l,VBM,a} - E_{l,CBM,a} = \Delta E_{VBM}(d_{1a},d_{1b})/\Delta\sigma_a - \Delta E_{CBM}(d_{1a},d_{1b})/\Delta\sigma_a = -4g_{z2}(\Delta d_{2z}/\Delta\sigma_a) \quad \text{(ES21)}$$

Based on the deformation potential $E_{l,VBM,a}$ and $E_{l,CBM,a}$ is -0.93 and -7.86 eV, we can conclude that the g_{z2} is times larger than k_π in value.

Obviously, the outstanding difference of $E_{l,VBM,a}$ and $E_{l,CBM,a}$ results from the highness-difference-sensitive p_z-p_z overlap determined by the significant change of d_{z2}.

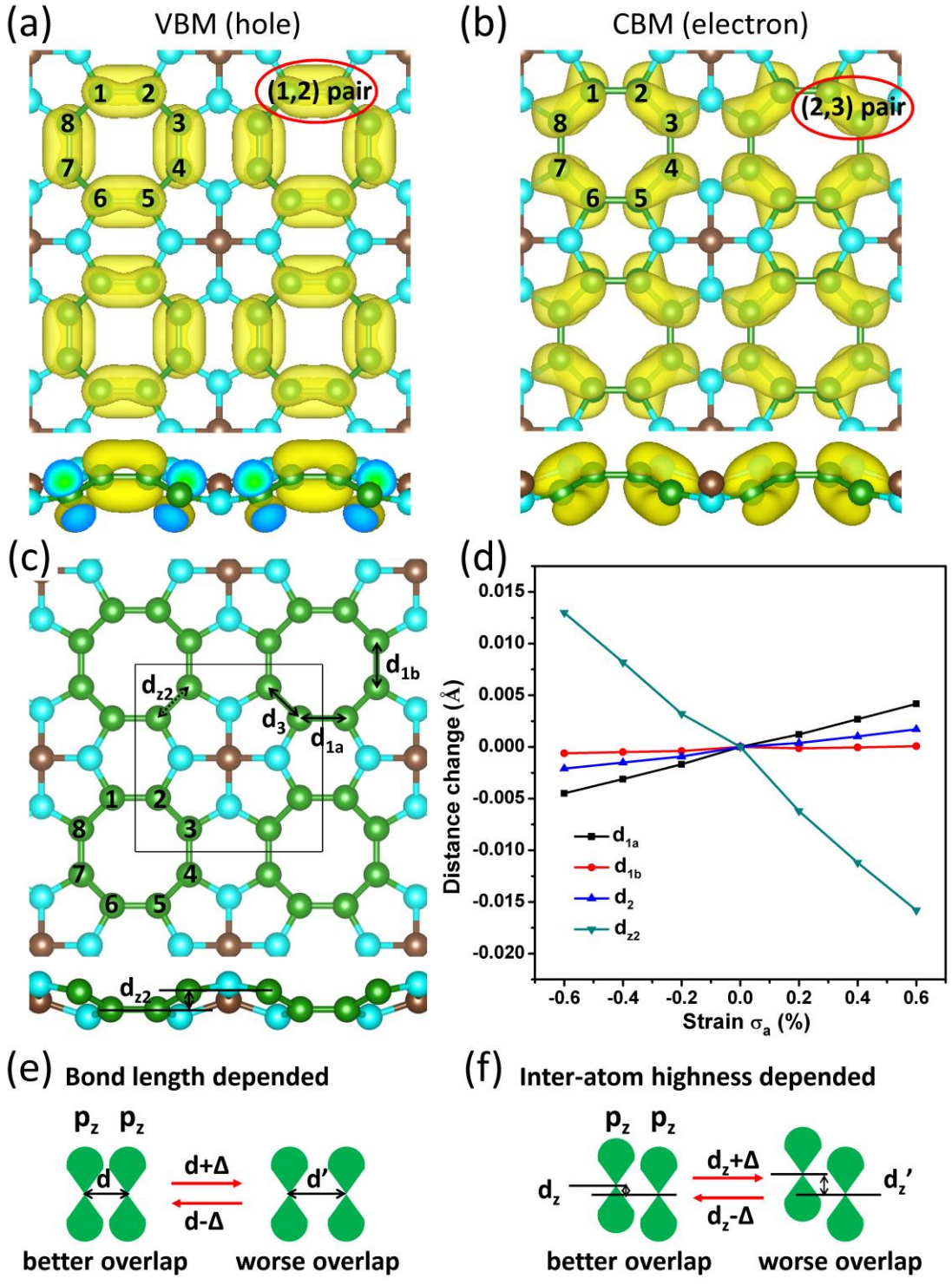

Fig. S9 (a) Partial density of VBM and (b) CBM; (c) the specific bond length (d_{1a}, d_{1b}, d_2) and atomic position highness difference (d_{z2}); (d) the change of d_{1a}, d_{1b}, d_2, and d_{z2} under uniaxial strain (from -0.6% to +0.6%) to obtain deformation potential; (e) bond length depended orbital coupling to form π bond by p_z and p_z orbitals; (f) inter-atom highness depended orbital coupling to form π bond by p_z and p_z orbitals.

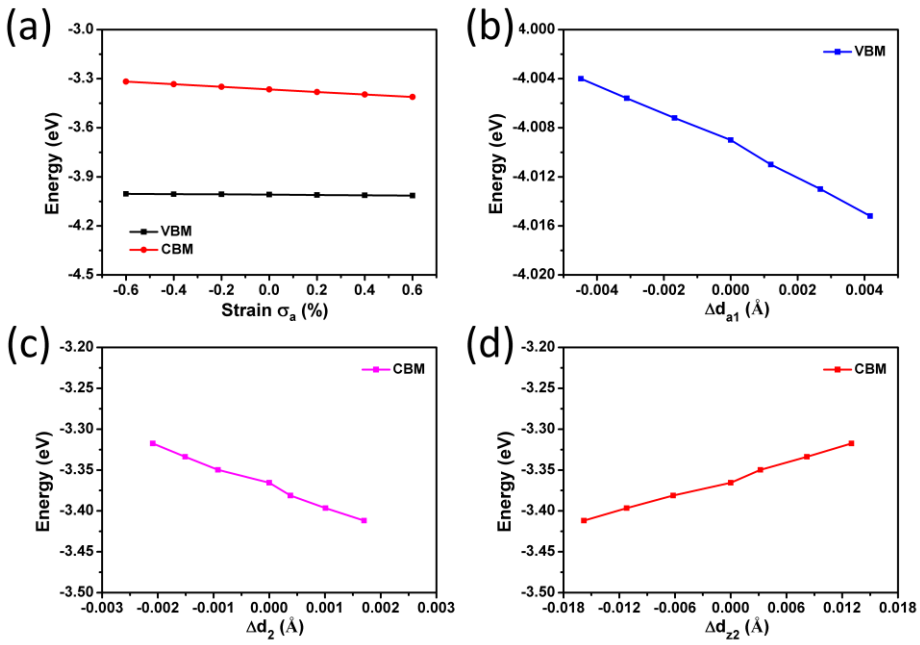

Fig. S10 (a) The energy of CBM and VBM under different strain (from -0.6% to +0.6%) to obtain deformation potential; (b) The energy of VBM in near-linear relationship with bond length change Δd_{a1}; (c) The energy of CBM in near-linear relationship with bond length change Δd_2; (d) The energy of CBM in near-linear relationship with inter-atom highness change Δd_{z2}.

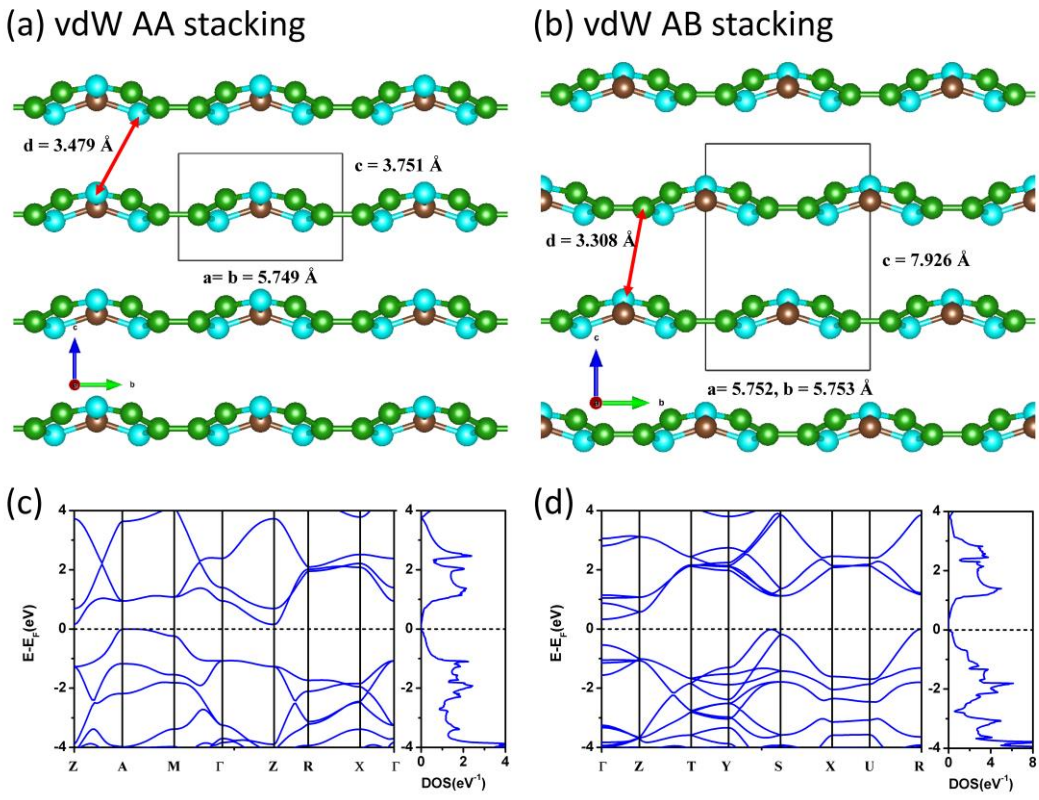

Fig. S11 Side views of structure of (a) AA and (b) AB stacking of Me-graphene vdW bulks. Black, blue and green balls represents C_1, C_2 and C_3 atom in Me-graphene, respectively. The band structure and DOS of (c) AA stacking and (d) AB stacking with DFT+D3.

GW calculation of layered bulks. Similar setting to monolayer is applied in bulk structure as well, except that the DFT-D3 was considered to treat their interlayered vdW interaction in layered bulk. For the two layered bulk structures, the GW0-D3 band gap is estimated to be 0.76 eV for AA stacking (k-points: 6×6×12) and 0.96 eV for AB stacking (k-points: 6×6×6).

References

1. L. Wang, A. Kutana, X. Zou and B. I. Yakobson, *Nanoscale*, 2015, **7**, 9746-9751.
2. G. Onida, L. Reining and A. Rubio, *Rev. Mod. Phys.*, 2002, **74**, 601-659.
3. L. Brus, *J. Phys. Chem.*, 1994, **98**, 3575-3581.
4. J. P. A. Charlesworth, R. W. Godby and R. J. Needs, *Phys. Rev. Lett.*, 1993, **70**, 1685-1688.
5. N. Berseneva, A. Gulans, A. V. Krasheninnikov and R. M. Nieminen, *Phys. Rev. B*, 2013, **87**, 035404.
6. M. Rohlfing and S. G. Louie, *Phys. Rev. B*, 2000, **62**, 4927-4944.
7. J.-H. Choi, P. Cui, H. Lan and Z. Zhang, *Phys. Rev. Lett.*, 2015, **115**, 066403.
8. M. Zhang, L.-Y. Huang, X. Zhang and G. Lu, *Phys. Rev. Lett.*, 2017, **118**, 209701.
9. J. Bardeen and W. Shockley, *Phys. Rev.*, 1950, **80**, 72-80.
10. G. Schusteritsch, M. Uhrin and C. J. Pickard, *Nano Lett.*, 2016, **16**, 2975-2980.